

UNIVERSIDAD DE LAS PALMAS DE GRAN CANARIA
FACULTAD DE CIENCIAS DEL MAR
DEPARTAMENTO DE FÍSICA



PROYECTO FINAL DE MÁSTER (TESINA):

WIND-DRIVEN CROSS-EQUATORIAL FLOW IN THE INDIAN OCEAN

MARÍA DOLORES PÉREZ HERNÁNDEZ

DIRECTOR: DR. ALONSO HERNÁNDEZ GUERRA

LAS PALMAS DE GRAN CANARIA A 3 DICIEMBRE DE 2010

Wind-driven Cross-Equatorial Flow in the Indian Ocean

M.DOLORES PÉREZ-HERNÁNDEZ * AND ALONSO HERNÁNDEZ-GUERRA

Facultad de Ciencias del Mar, Universidad de Las Palmas de Gran Canaria, Las Palmas, Spain

TERRENCE M. JOYCE

Department of Physical Oceanography, Woods Hole Oceanographic Institution, Woods Hole, USA

PEDRO VÉLEZ-BELCHÍ

Instituto Español de Oceanografía, Avenida Tres de Mayo, Santa Cruz de Tenerife, Spain

* *Corresponding author address:* Dr. Terrence Joyce, Woods Hole Oceanographic Institution, Woods Hole, MA 02543.

E-mail: latex@ametsoc.org

ABSTRACT

NCEP Wind-stress and temperature and salinity data from Argo have been used together with a steady model to estimate the meridional velocity and volume and heat transport in the Equatorial Indian Ocean for a seven years period (2003-2009). Total volume transport of the wind stress curl shows a northward and southward flow for the Winter and Summer Monsoon, respectively. The velocity section shows a Somali Current flowing in opposite direction in the Winter and Summer Monsoons. In the Winter Monsoon, the Somali Current is shallow (~ 200 dbar) and flows to the south with an undercurrent below it. In the Summer Monsoon and Transitional Periods, the Somali Current flows to the north and to the south, respectively and extend to (~ 650 dbar) depth. The heat transport across the Equator presents a seasonal reversing, being -0.8 PW to the south in the Winter monsoon and $+1.2$ PW in the Summer Monsoon. The annual heat transport is -1.4 PW that is mainly carried out by the Somali Current.

1. Introduction

Indian Ocean is under the influence of the Winter and Summer Monsoons. Both monsoons represent very different wind and ocean circulation conditions (Reppin et al. 1999; Grumet et al. 2002; Tomczak and Godfrey 2003). The Winter or Northeast Monsoon prevails during the months of December, January, February and March (Schott et al. 1990; Donguy and Meyers 1995; Grumet et al. 2002; Tomczak and Godfrey 2003). During this period, trade winds of the northern hemisphere (Figure 1) cover the northern Indian Ocean down to approximately 10° S, generating a wind-driven southward Somali Current (Western Boundary Current) (Reppin et al. 1999; Schott et al. 2001). The interior flow is considered to run northward in this season (Levitus 1988; Schott et al. 2001). In this study, we refer as season every monsoon and the Transitional periods.

The Summer or Southwestern Monsoon stands on the months of June, July, August and September (Schott et al. 2001; Grumet et al. 2002; Tomczak and Godfrey 2003; Shenoi et al. 2009). This monsoon is characterized by strong southwesterly winds (Figure 1), which are considered to be a northward propagation of the southern hemisphere trade winds (Tomczak and Godfrey 2003). This strong wind occupies the whole Indian Ocean reversing the northern hemisphere situation. The Somali Current, due to its wind-driven character, runs northward during this monsoon (Reppin et al. 1999; Grumet et al. 2002). In the rest of the equatorial area, a southward transport is found (Levitus 1988; Schott et al. 2001).

In between both monsoons, two transitional periods occur. The first one involves the months of April and May and the second one occurs in October and November (Reppin et al. 1999; Murty et al. 2000; Schott et al. 2001; Tomczak and Godfrey 2003; Shenoi et al. 2009).

The wind during those periods has a very weak meridional component and a strong zonal component (Hastenrath and Lamb 2004). The first Transitional Period makes the transition from Winter to Summer Monsoon. At this time the meridional flow is determined by the Somali Current which is still being southward (Donguy and Meyers 1995). The second period is the Summer to Winter Monsoon transition. In these months, Somali Current continues the northward Summer Monsoon flow carrying waters across the Equator (Donguy and Meyers 1995).

The oceanic regime in the Indian Ocean has yielded into several studies by areas and periods (Duing et al. 1980; Leetmaa et al. 1980; Luyten et al. 1980; Schott and Quadfasel 1982; Schott et al. 1990; Donguy and Meyers 1995; Reppin et al. 1999; Murty et al. 2000). Schott et al. (2001) presents a review of the previous studies carried out in the Indian Ocean. It is worth to mention that the zonal current in the equatorial Indian Ocean has been deeply studied (Wyrtki 1973; Knox 1976; Reppin et al. 1999; Hastenrath 2000; Sengupta et al. 2007) but the studies about the Cross-Equatorial flow in the Indian Ocean have been focused on the western boundary Somali Current (Leetmaa et al. 1980; Duing et al. 1980; Leetmaa et al. 1982; Schott et al. 1990; Grumet et al. 2002). Most of them are in situ studies done with current meters and lagrangian drifters at different periods with the aim of studying the intensity and the reversal of the Somali Current.

In the study of the Cross-Equatorial circulation, Joyce (1988a) proposed that wind and dynamic height present a dynamical balance across the Equator that permits the formation of a Cross-Equatorial flow. This idea was based on the Sverdrup (1947) study which suggested that the meridional pressure gradient could be balanced by meridional wind-stress. The resulting steady-state equations transform the initial Navier-Stokes equations by expanding

them into a Taylor series at the Equator. This takes into account the equatorial β -plane, which considers the Coriolis force as $f = \beta y$, being $\beta = f_y$ at the Equator and y the meridional axis.

The equations proposed by Joyce (1988a) evaluated at the Equator are the following:

$$\tau_z^y = P_y \quad (1)$$

$$-\beta \tilde{v} = (\tau_{yz}^x - \tau_{xz}^y) / \rho_0 = (\tau_{yz}^x - P_{xy}) / \rho_0 \quad (2)$$

$$\tilde{v} = v(1 - u_{yy} / \beta) \quad (3)$$

Equation (1) shows that the vertical variation of the meridional wind stress (τ_z^y) balances the meridional pressure gradient (P_y). Equation (2) reflects the Sverdrup balance with a modified meridional velocity (\tilde{v}), and equation (3) is just the relation between the meridional velocity (v) and the modified meridional velocity obtained by (2). These are linearized equations that consider $u_y = 0$ and $w_y = 0$ at the Equator. This means that the Equator is an extremum in zonal and vertical velocities. Singular to the Indian Ocean, strong zonal equatorial velocities occur in the Transitional Periods called Wyrтки jet (Wyrтки 1973). In the other seasons zonal currents decrease significantly, being close to zero (Knox 1976). The extremum in vertical velocity is more difficult to demonstrate due to the lack of in situ studies. Several evidences has shown that, in contrast to the other equatorial regimes, the upwelling at the Equator in the Indian Ocean is absent due to the meridional orientation of the winds and therefore $w = 0$ (Schott et al. 2001, 2002; Tomczak and Godfrey 2003; Diansky et al. 2006). This model has already been used by Joyce (1988a,b) to study the volume and heat transport and the meridional velocities across the equatorial Pacific and

Atlantic Oceans.

The aim of this paper is to investigate the Indian Ocean Cross-Equatorial meridional velocities and transport of volume and heat per season using the above wind-driven model proposed by Joyce (1988a,b). For this purpose, hydrographic data come from the Argo International Program and winds from the National Centres for Environmental Prediction (NCEP) Reanalysis Project.

2. Data and Methods

Wind and hydrographic data for a seven years period (2003 and 2009) are collected for the geographic area between 44.5° to 96° E. The westernmost longitude is imposed by the slant of the Somali coast. The latitude range is 2.5° and 4° at both sides of the Equator, for wind and hydrographic data, respectively. The average of 7 years of wind data avoids the strong interannual variability found in the Indian equatorial ocean (Barnett 1983; Reverdin 1987). Due to the strong time variability along a year found in the equatorial Indian Ocean, we have considered three different seasons to carry out this study: Winter Monsoon (December-March), Summer Monsoon (June-September) and Transitional Periods. Transitional periods are considered together because there are not enough profiles to considerer them separately.

The wind data comes from the National Centers for Environmental Prediction (NCEP) Reanalysis Project form the National Oceanic and Atmospheric Administration (NOAA). This Project produces new analyses of atmospheric condition using historical data. Wind data were downloaded every 2.5° of latitude and longitude per month and year. These data were average per season. Wind stress (Figure 1 is 2) are calculated with the quadratic

relationship proposed by Large and Pond (1981).

Hydrographic data comes from the Argo International Program. The Program consists on profilers launched around the world. These profilers descend to the parking depth (usually 1500 m). Every 10 days they descend to 2000 m and then they ascend up to the surface measuring salinity and temperature at discrete depths. Once in the surface, they transmit those data to the Coriolis data Centre via the Global Telecommunications Systems (GTS). Once data have been checked, this Centre provides a grey list that contains the wrong profiles. We have removed these wrong profiles from our data base and others that were considered anomalous after a visual inspection of them. The visual inspection consists in the comparison between neighbor profiles excluding those with wrong behavior in temperature or salinity. The amount of profilers per season used in this study is shown in Figure 3 (9839 profiles in total: 3537 for the Winter Monsoon, 3186 for the Transitional Periods and 3116 for the Summer Monsoon).

An objective analysis has been made by season to interpolate data into a regularly spaced grid every 2.5° in longitude and 0.5° in latitude. Objective analysis is an optimal statistical interpolation by means of successive corrections (Pedder 1993). It is commonly used to obtain climatological fields, as it is designed to minimize the noise-to-signal ratio. Noise is defined as any non-resolved scale, and in transoceanic sections it is mainly attributed to eddies. This method has been previously used by Fraile-Nuez and Hernández-Guerra (2006); Hernández-Guerra et al. (2009); Vélez-Belchí et al. (2010) for Argo data. World Ocean Atlas 2005 (WOA05) climatology data averaged per season are used as first guess to ensure that the anomaly field (data minus climatology) is a stationary, zero-mean random function of the location. WOA05 field is composed by monthly salinity and temperature data from the

surface down to 1500 m and annual data from 1500 m to 2000 m.

In order to evaluate the steady-state model, we have to compute meridional and zonal gradients. Meridional gradients are calculated by least square fits between -2.5 and 2.5 degrees. For wind stress, we have only three values but eleven values for dynamic height. Zonal gradients are estimated by differencing wind stress and dynamic height over 2.5 degree of longitude.

Figure 4 shows the objective analyzed vertical sections of temperature (left column) and salinity (right column) over the equatorial Indian Ocean for each season. Above the seasonal thermocline (~ 200 m), a shallow layer of different temperature and salinity values are found. These are due to the seasonal heating, evaporation, and eventually low salinity waters advected from the Bay of Bengal and Indonesian Throughflow where river discharge and precipitation takes relevance. From 70° E to the eastern most side, low salinities and high temperatures indicates the presence of Bay of Bengal Water (BBW), which spreads on a thick layer of ~ 100 m (You and Tomczak 1993; Tomczak and Godfrey 2003). Below the seasonal thermocline, Indian Central Water (ICW) and Australasian Mediterranean Water (AAMW) are found. ICW dominates practically the whole section with salinities between 35 and 35.2, being thinner to the east. The AAMW enters from the Indonesian Throughflow as a front into the equatorial area, with temperatures around 8° C and salinities below 35 in a depth range from ~ 300 to ~ 1100 m (Tomczak and Large 1989; You and Tomczak 1993). It is clearly seen in the vertical section of salinity that this water mass forms patches at the depth of ICW in the western side of the basin. Below the 1500 dbar, Indian Deep Water (IDW) is observed with salinities around 34.8 (Tomczak and Godfrey 2003).

3. Results and Discussion

a. Model

As stated in Equation (1), there should be a balance between the pressure gradients and the frictional forces created by Cross-Equatorial winds at the Equator. To examine this balance, the meridional pressure gradients at the surface relative to 1000 m depth and the meridional wind stress at each season are presented in Figures 5 and 6, respectively. The correspondence between both slopes is apparent except in a few longitudes. This is due to the mesoscale signal present in the hydrographic data. Objective analysis reduces the mesoscale signal but they are still present in the data. High mesoscale signal in the meridional component of the velocity at the equatorial Indian Ocean at 80.5° E is clearly seen from ADCP data shown in Reppin et al. (1999). Meridional velocity reversing from positive to negative is shown in their plate 1 with a much shorter time scale than the zonal velocity.

To analyze Equation (1) further, the vertically integrated gradient of the dynamic height is calculated at different reference pressures and compared with the meridional wind stress (Figure 7). The lower limit of integration is different for each season. Different behaviors are seen in each season which requires the use of different y-axis. The Winter Monsoon (Figure 7 top) presents a negative and a increasing meridional wind stress from east to west to roughly 50° E, as the integrated meridional gradient of the dynamic height, although a mesoscale signal is clearly seen in the hydrographic data. At 50° E, there is a change in the slope of the meridional wind stress that is also presumably presented in the meridional gradient of the dynamic height although the presence of the eddy signal makes difficult to

confirm it. For the Transitional Periods (Figure 7 middle), meridional wind stress is weak from the east to 50° E where a stronger positive wind stress starts. The integrated meridional gradient of the dynamic height roughly follows this behavior. The meridional wind stress of the Summer Monsoon (Figure 7 bottom) nearly resembles that of the Winter Monsoon but in an opposite way. On this occasion, the wind stress is positive and monotonic increasing from 70° E to the western boundary. The integrated meridional gradient of the dynamic height roughly follows this same pattern.

b. Volume Transport

Both components and the total of the volume transport from the wind-stress curl together with the accumulated volume transport are plotted in Figures 8 to 10 for each season. The component τ_x^y fluctuates about zero for the three seasons, just like at the equatorial Pacific and Atlantic Oceans (Joyce 1988a,b). The integrated transport for this component of the wind-stress curl is 0.5 Sv, -1.1 Sv and -3.1 Sv ($1 \text{ Sv} = 10^6 \text{ m}^3 \text{ s}^{-1}$) for the Winter Monsoon, Transitional Periods and Summer Monsoon, respectively. It is worth to mention that this component of the wind-stress curl changes sign when approaching the western boundary, more apparent in the Winter and Summer Monsoons. The equatorial $-\tau_y^x$ component for the Winter and Summer Monsoons has different directions, northward and southward, respectively. The magnitude of the accumulated volume transport for this component of the wind-stress curl in the Summer Monsoon is larger (-7.2 Sv) than in the Winter Monsoon (3.0 Sv). The Transitional Periods has a very weak southward transport of -1.0 Sv and located in the eastern half of the Indian Ocean. The total wind-stress curl integrated west-

ward from the eastern boundary shows a roughly monotonic increase (absolute value) in the Winter and Summer Monsoon until approaching the western boundary where an inflection of the total volume transport is observed. For the Transitional Periods, only the eastern and western boundaries show a remarkable volume transport. Table 1 shows the volume transport for each component of the wind-stress curl and the total for each season. The annual integrated volume Transport in the equatorial Indian Ocean is -8.9 Sv, very close to the Atlantic Ocean integrated volume transport (Joyce 1988b), which is an indicator of the strength of the wind stress curl in the Equatorial Indian Ocean, despite of its reverses.

We have also used QuickScat winds collected from satellite data. Volume transports computed are much higher than those obtained from NCEP data. Using QuickScat wind data, the integrated total volume transport is 20 Sv, -8 Sv and -23 Sv for Winter Monsoon, Transitional Periods and Summer Monsoon, respectively. Therefore, volume transport from QuickStat data is in the range 3.3-5.7 higher than that obtained from NCEP products. Anyway, volume transports corresponding to each wind products present a similar behaviour: northward flow in the Winter Monsoon, negative in the Transitional Periods and Summer Monsoon, being the volume transport in the Transitional Periods lower than in the Summer Monsoon. Different results using various wind data products have been previously documented in Schott et al. (2001).

The vertical transport is calculated from the objectively analyzed Argo data using the fact that $\tau_{xz}^y = P_{xy}$. The reference level is chosen as that the volume transport from P_{xy} matches that from τ_{xz}^y . For the Winter Monsoon, the reference layer is 800 dbar although 200 dbar also gives the same volume transport. In the Transitional Periods and Summer Monsoon, the reference layer is found at 680 and 640 dbar, respectively. Table 1 shows

the vertically integrated transport for P_{xy} . Figures 11, 12, 13 shows the zonal integrated vertical profile for the frictional term determined from the winds, the vertical profile from the hydrographic data and the total for the Winter Monsoon, Transitional Periods and Summer Monsoon, respectively. The frictional term is assumed to have an exponential decay from the sea surface with an e-folding distance of 100 dbar as in Joyce (1988a).

In the Winter Monsoon and Transitional Periods, there is a total southward flow in the 200 and 680 dbar, respectively, arising from P_{xy} (Figures 11, 12). In contrast, Summer Monsoon presents a northward transport in the first 640 dbar also arising from P_{xy} (Figure 13). In every season, there is a deep flow opposites to the surface transport to satisfy volume transport constraint.

c. Meridional Velocities

Meridional Velocities, \tilde{v} , were obtained using Equation (2) and represented in figures 14, 15 and 16 for each season. Reference pressure levels were chosen according to Equation (1), being 800 dbar for the Winter Monsoon, 680 dbar for the Transitional Periods and 640 dbar for the Summer Monsoon, as already mentioned. Indian ocean has higher meridional velocities than the equatorial Atlantic and Pacific Oceans during the whole year (Joyce 1988a,b; Tomczak and Godfrey 2003).

On the western boundary, the Somali Current is clearly seen in each season. In the Winter Monsoon and Transitional Periods, it flows southward with velocities higher than -30 cm s^{-1} and -20 cm s^{-1} , respectively. In contrast, on the Summer Monsoon the Somali Current reverses flowing northward with stronger velocities higher than 40 cm s^{-1} . Leetmaa

et al. (1982) using in situ data documents this reversing flow between the Transitional Period in April and early May and the Summer Monsoon during the onset of southerly winds. The structure of the Somali Current is quite different for each season. For the Winter Monsoon, it is confined in the first 200 dbar and western of 50° E, when is the nearest to the coast (Diansky et al. 2006). The volume transport of the Somali Current in this season is -25.6 Sv. Below ~ 200 m an undercurrent is clearly observed to ~ 700 m depth with velocities under 10 cm s^{-1} that results a northward transport of 8.6 Sv. This gives a Somali Current total transport of -17.0 Sv southward. This picture of a Somali Current flowing to the south and an undercurrent flowing to the north in the Winter Monsoon was previously detected by Schott (1986) and Schott et al. (1990) being the only season with this pattern as observed in Figures 14 to 16. The difference between Schott et al. (1990) results and ours is that they found a thinner surface layer flowing to the south (<120 m) and the undercurrent spanned to 400 m depth. The pattern of higher velocities in the Summer than in the Winter Monsoon were also reported by Schott et al. (1990).

In the Transitional Periods, the Somali Current spreads down to 670 dbar and offshore transporting -33.6 Sv southward. In the Summer Monsoon, the Somali Current presents its maximum velocity in the surface layer and it spreads down to the reference layer. On this season, the Somali Current transports 38.9 Sv northward.

The difference transport across the equator of the Somali Current being larger in the Summer Monsoon (38.9 Sv) than in Winter Monsoon (-17.0 Sv) has also been reported by Schott et al. (1990) although with a smaller transport. This discrepancy is explained by the different offshore measurements of the Somali Current. Schott et al. (1990) installed a moored array to $\sim 44.5^\circ$ E, a western longitude to the Somali Current offshore extension seen

in our data. If we compute the transport of the Somali Current in the first longitude interval closest to the Somali coast, results -3.9 Sv in the Winter Monsoon that is roughly similar to the reported by Schott et al. (1990) that was -1.1 Sv. If same calculations are carried out for the other seasons, we get -19.8 Sv for the Transitional Period about to the -21 Sv obtained by Quadfasel and Schott (1982) and +29.1 Sv for the Summer Monsoon closer to the 21.1 Sv shown in Schott et al. (1990). Our results show an annual net northward transport of +5.4 Sv that again roughly matches the +10.5 Sv obtained by Schott et al. (1990).

d. Heat Transport

We have used our results to estimate the heat transported by the Indian Ocean across the equator. In this estimation, we have neglected the transport balance that has not been found in our data and the heat transport deeper than 2000 m. However, with our data we can find out if the heat transport changes seasonally.

Table 2 shows the heat transported by the Somali Current, the ocean interior and the net for the Winter Monsoon, the Transitional Periods, the Summer Monsoon and the annual. The annual heat transport has been calculated as the sum of the heat transport in each season.

As seen in Table 2, the heat transport across the equator of the Indian Ocean in every season has different direction for the Somali Current and the ocean interior. The net heat transport has the same direction as the heat transported by the Somali Current. The Somali Current transports heat to the south in the Winter Monsoon (-2.1 PW, $1 PW = 10^{15} W$) and Transitional Periods (-2.2 PW) and to the north in the Summer Monsoon (+2.9 PW).

The southward heat transport of the Somali Current in the Winter Monsoon agrees with the estimation provided by Schott et al. (1990). In contrast, the heat transport carried out by the ocean interior is to the north in the Winter Monsoon (+1.3PW) and Transitional Periods (+0.4PW) and to the south in the Summer Monsoon (-1.7PW). Then, the net seasonal heat transport is -0.8PW in the Winter Monsoon, -1.8PW in the Transitional Periods and +1.2PW in the Summer Monsoon.

We have attempted to compare our seasonal heat transport estimation with previous studies using different methodology. Surprising, our estimations do not match even in the direction with the measurements provided by these studies. Wacongne and Pacanowski (1996) found that the heat transport in the Winter and Summer Monsoon is +1.0PW and -1.2PW, respectively. These transports agree with those estimates by different authors (Hsiung et al. 1989; Hastenrath and Greischar 1993; Chirokova and Webster 2006). However, these heat transports are of the order of magnitude of the heat transport of the ocean interior as seen in Table 2.

The annual heat transport is -1.4PW across the equator (Table 2) in agreement with the estimation of Hsiung (1985) although the magnitude of our estimate is about twice as large. Anyway, Hsiung (1985)'s estimation is also about twice larger than the provided by Hastenrath (1982). If we consider that the water transport below 2000m depth is to the north in the Indian Ocean as seen in Ganachaud and Wunsch (2000), our estimation of heat transport would decrease and, therefore, being closer to that estimated by Hsiung (1985). Results from our data as seen in Table 2 is that the annual heat transport corresponds to the heat transported by the Somali Current. The annual heat transport of the ocean interior is not significant.

Acknowledgments.

Hydrographic data were collected and made freely available by the International Argo project (<http://www.argo.net>). The wind field were obtained from the National Centers for Environmental Prediction (NCEP) Reanalysis Project (<http://www.cpc.ncep.noaa.gov/products/wesley/reanalysis.html>) from the National Oceanic and Atmospheric Administration (NOAA). This study has been partly funded by the MOC project (CTM 2008-06438), financed by the Spanish Government and Feder.

REFERENCES

- Barnett, T., 1983: Interaction of the monsoon and Pacific trade wind system at interannual time scales Part I: The equatorial zone. *Monthly Weather Review*, **111** (4), 756–773.
- Chirokova, G. and P. Webster, 2006: Interannual variability of Indian Ocean heat transport. *Journal of Climate*, **19**, 1013–1031.
- Diansky, N., V. Zalesny, S. Moshonkin, and A. Rusakov, 2006: High resolution modeling of the monsoon circulation in the Indian Ocean. *Oceanology*, **46** (5), 608–628.
- Donguy, J. and G. Meyers, 1995: Observations of geostrophic transport variability in the western tropical Indian Ocean. *Deep Sea Research Part I: Oceanographic Research Papers*, **42** (6), 1007–1028.
- Duing, W., R. Molinari, and J. Swallow, 1980: Somali current: Evolution of surface flow. *Science*, **209** (4456), 588.
- Fraille-Nuez, E. and A. Hernández-Guerra, 2006: Wind-driven circulation for the eastern North Atlantic Subtropical Gyre from Argo data. *Geophysical Research Letters*, **33** (3), L03 601.
- Ganachaud, A. and C. Wunsch, 2000: Improved estimates of global ocean circulation, heat transport and mixing from hydrographic data. *Nature*, **408** (6811), 453–457.

- Grumet, N., T. Guilderson, and R. Dunbar, 2002: Meridional transport in the Indian Ocean traced by coral radiocarbon. *Journal of Marine Research*, **60** (5), 725–742.
- Hastenrath, S., 1982: On meridional heat transports in the world ocean. *Journal of Physical Oceanography*, **12** (8), 922–927.
- Hastenrath, S., 2000: Zonal circulations over the equatorial Indian Ocean. *Journal of Climate*, **13** (15), 2746–2756.
- Hastenrath, S. and L. Greischar, 1993: The monsoonal heat budget of the hydrosphere-atmosphere system in the Indian Ocean sector. *Journal of Geophysical Research*, **98** (C4), 6869–6881.
- Hastenrath, S. and P. Lamb, 2004: Climate dynamics of atmosphere and ocean in the equatorial zone: a synthesis. *International Journal of Climatology*, **24** (13), 1601–1612.
- Hernández-Guerra, A., T. Joyce, E. Fraile-Nuez, and P. Velez-Belchí, 2009: Using Argo data to investigate the meridional overturning circulation in the North Atlantic. *Deep Sea Research Part I: Oceanographic Research Papers*.
- Hsiung, J., 1985: Estimates of global oceanic meridional heat transport. *Journal of physical oceanography*, **15** (11), 1405–1413.
- Hsiung, J., R. Newell, and T. Houghtby, 1989: The annual cycle of oceanic heat storage and oceanic meridional heat transport. *Quarterly Journal of the Royal Meteorological Society*, **115** (485), 1–28.

- Joyce, T., 1988a: Wind-driven cross-equatorial flow in the Pacific Ocean. *Journal of Physical Oceanography*, **18** (1), 19–24.
- Joyce, T., 1988b: On the wind-driven cross-equatorial flow in the Atlantic Ocean. *Journal of Physical Oceanography*, **18** (5), 793–799.
- Knox, R., 1976: On a long series of measurements of Indian Ocean equatorial currents near Addu Atoll. *Deep Sea Research and Oceanographic Abstracts*, Elsevier, Vol. 23, 211–221.
- Large, W. and S. Pond, 1981: Open ocean momentum flux measurements in moderate to strong winds. *Journal of physical oceanography*, **11** (3), 324–336.
- Leetmaa, A., D. Quadfasel, and D. Wilson, 1982: Development of the flow field during the onset of the Somali Current, 1979. *Journal of Physical Oceanography*, **12** (12).
- Leetmaa, A., H. Rossby, P. Saunders, and P. Wilson, 1980: Subsurface circulation in the Somali Current. *Science*, **209** (4456), 590.
- Levitus, S., 1988: Ekman volume fluxes for the world ocean and individual ocean basins. *Journal of Physical Oceanography*, **18** (2), 271–279.
- Luyten, J., M. Fieux, and J. Gonella, 1980: Equatorial currents in the western Indian Ocean. *Science*, **209** (4456), 600.
- Murty, V., et al., 2000: Seasonal variability of upper-layer geostrophic transport in the tropical Indian Ocean during 1992-1996 along TOGA-I XBT tracklines. *Deep Sea Research Part I: Oceanographic Research Papers*, **47** (8), 1569–1582.

- Pedder, M., 1993: Interpolation and filtering of spatial observations using successive corrections and Gaussian filters. *Monthly Weather Review*, **121** (10), 2889–2902.
- Quadfasel, D. and F. Schott, 1982: Water-mass distributions at intermediate layers off the Somali coast during the onset of the southwest monsoon, 1979. *Journal of Physical Oceanography*, **12** (12), 1358–1372.
- Reppin, J., F. Schott, J. Fischer, and D. Quadfasel, 1999: Equatorial currents and transports in the upper central Indian Ocean: Annual cycle and interannual variability. *Journal of Geophysical Research*, **104** (C7), 15 495.
- Reverdin, G., 1987: The Upper Equatorial Indian Ocean. The Climatological Seasonal Cycle. *Journal of Physical Oceanography*, **17** (7), 903–927.
- Schott, F., 1986: Seasonal variation of cross-equatorial flow in the Somali Current. *Journal of Geophysical Research*, **91** (C9), 10 581.
- Schott, F., M. Dengler, and R. Schoenefeldt, 2002: The shallow overturning circulation of the Indian Ocean. *Progress in oceanography*, **53** (1), 57–103.
- Schott, F., J. McCreary, et al., 2001: The monsoon circulation of the Indian Ocean. *Progress in Oceanography*, **51** (1), 1–123.
- Schott, F. and D. Quadfasel, 1982: Variability of the Somali Current system during the onset of the southwest monsoon, 1979. *J. Phys. Oceanogr.:(United States)*, **12** (12).
- Schott, F., J. Swallow, and M. Fieux, 1990: The Somali Current at the equator: Annual cycle

- of currents and transports in the upper 1000 m and connection to neighbouring latitudes. *Deep Sea Research Part A. Oceanographic Research Papers*, **37 (12)**, 1825–1848.
- Sengupta, D., R. Senan, B. Goswami, and J. Vialard, 2007: Intraseasonal variability of equatorial Indian Ocean zonal currents. *Journal of Climate*, **20 (13)**, 3036–3055.
- Shenoi, S. Nasnodkar, N. Rajesh, I. G. Jossie Joseph, K. Suresh, and A. Almeida, 2009: On the diurnal ranges of Sea Surface Temperature (SST) in the north Indian Ocean. *Journal of Earth System Science*, **118**, 483–496.
- Sverdrup, H., 1947: Wind-driven currents in a baroclinic ocean; with application to the equatorial currents of the eastern Pacific. *Proceedings of the National Academy of Sciences of the United States of America*, **33 (11)**, 318.
- Tomczak, M. and J. Godfrey, 2003: *Regional oceanography: an introduction*. Daya Books.
- Tomczak, M. and D. Large, 1989: Optimum multiparameter analysis of mixing in the thermocline of the eastern Indian Ocean. *Journal of Geophysical Research*, **94 (C11)**, 16 141.
- Vélez-Belchí, P., A. Hernández-Guerra, E. Fraile-Nuez, and V. Benítez-Barrios, 2010: Changes in the temperature and salinity tendencies of the upper subtropical North Atlantic Ocean at 24.5N. *Journal of Physical Oceanography (in press)*.
- Wacongne, S. and R. Pacanowski, 1996: Seasonal heat transport in a primitive equations model of the tropical Indian Ocean. *Journal of physical oceanography*, **26 (12)**, 2666–2699.
- Wyrtki, K., 1973: An equatorial jet in the Indian Ocean. *Science*, **181 (4096)**, 262.

You, Y. and M. Tomczak, 1993: Thermocline circulation and ventilation in the Indian Ocean derived from water mass analysis. *Deep Sea Research Part I: Oceanographic Research Papers*, **40 (1)**, 13–56.

List of Tables

- 1 Volume transport (Sv) per season. Every row shows the transport for each component of the wind stress curl and from hydrography. The total shows two results considering the curl of the wind stress and the hydrography 23
- 2 Heat transport (PW) per season and annual. The first row shows the heat transport due to the Somali Current, while the second row is the ocean interior contribution. Net heat transport per season can be found at the end of each column 24

TABLE 1. Volume transport (Sv) per season. Every row shows the transport for each component of the wind stress curl and from hydrography. The total shows two results considering the curl of the wind stress and the hydrography

	<i>Winter Monsoon</i>	<i>Transitional Periods</i>	<i>Summer Monsoon</i>
τ_x^y	0.5	-1.1	-3.1
P_{xy}	0.5	-1.2	-1.1
τ_y^x	3.0	-1.0	-7.2
Total	3.5/3.5	-2.1/-2.2	-10.3/-8.3

TABLE 2. Heat transport (PW) per season and annual. The first row shows the heat transport due to the Somali Current, while the second row is the ocean interior contribution. Net heat transport per season can be found at the end of each column

	<i>Winter Monsoon</i>	<i>Transitional Periods</i>	<i>Summer Monsoon</i>	<i>Annual</i>
<i>SomaliCurrent</i>	-2.1	-2.2	2.9	-1.4
<i>Oceaninterior</i>	1.3	0.4	-1.7	0
<i>Net</i>	-0.8	-1.8	1.2	-1.4

List of Figures

- 1 Wind stress field in the Winter Monsoon (top), Transitional periods (middle) and Summer Monsoon (bottom). 27
- 2 Zonal (top) and Meridional (bottom) wind stress at the Equator in the Winter Monsoon (left), Transitional Peridiods (middle), and Summer Monsoon (right) 28
- 3 Distribution of Argo floats over the equatorial Indian Ocean in each season. Colors represent the year of each profile. 29
- 4 Temperature (left column) and Salinity (right column) vertical sections in each season. 30
- 5 Surface dynamic height relative to 1000 m depth (in dynamic meters) at selected longitudes across the equatorial Indian Ocean for each season. 31
- 6 Meridional wind stress (in Pa) at selected longitudes across the equatorial Indian Ocean for each season. 32
- 7 Meridional wind stress (solid line) and integrated meridional gradient of the dynamic height at different pressure references (dashed lines) along the equatorial Indian Ocean. Each season has a different y-scale and pressure references. 33
- 8 Zonal distribution (left) and accumulated from the eastern boundary (right) volume transport of each component of the wind stress curl and total corresponding to the Winter Monsoon. 34
- 9 Zonal distribution (left) and accumulated from the eastern boundary (right) volume transport of each component of the wind stress curl and total corresponding to the Transitional Periods. 35

- 10 Zonal distribution (left) and accumulated from the eastern boundary (right) volume transport of each component of the wind stress curl and total corresponding to the Summer Monsoon. 36
- 11 Zonal integral of the volume transport from the surface to 2000 dbar every 50 dbar for $-\tau_{yz}^x$ (left), P_{xy} (middle) and total (right) for the Winter Monsoon. 37
- 12 Zonal integral of the volume transport from the surface to 2000 dbar every 50 dbar for $-\tau_{yz}^x$ (left), P_{xy} (middle) and total (right) for the Transitional Periods. 38
- 13 Zonal integral of the volume transport from the surface to 2000 dbar every 50 dbar for $-\tau_{yz}^x$ (left), P_{xy} (middle) and total (right) for the Summer Monsoon. 39
- 14 Vertical section of meridional velocities (in $cm s^{-1}$) at the equatorial Indian Ocean in the Winter Monsoon. Negative velocities are cross-hatched. The isolines interval is 5 to $10 cm s^{-1}$ and $10 cm s^{-1}$ afterwards. 40
- 15 Vertical section of meridional velocities (in $cm s^{-1}$) at the equatorial Indian Ocean in the Transitional Periods. Negative velocities are cross-hatched. The isolines interval is 5 to $10 cm s^{-1}$ and $10 cm s^{-1}$ afterwards. 41
- 16 Vertical section of meridional velocities (in $cm s^{-1}$) at the equatorial Indian Ocean in the Summer Monsoon. Negative velocities are cross-hatched. The isolines interval is 5 to $10 cm s^{-1}$ and $10 cm s^{-1}$ afterwards. 42

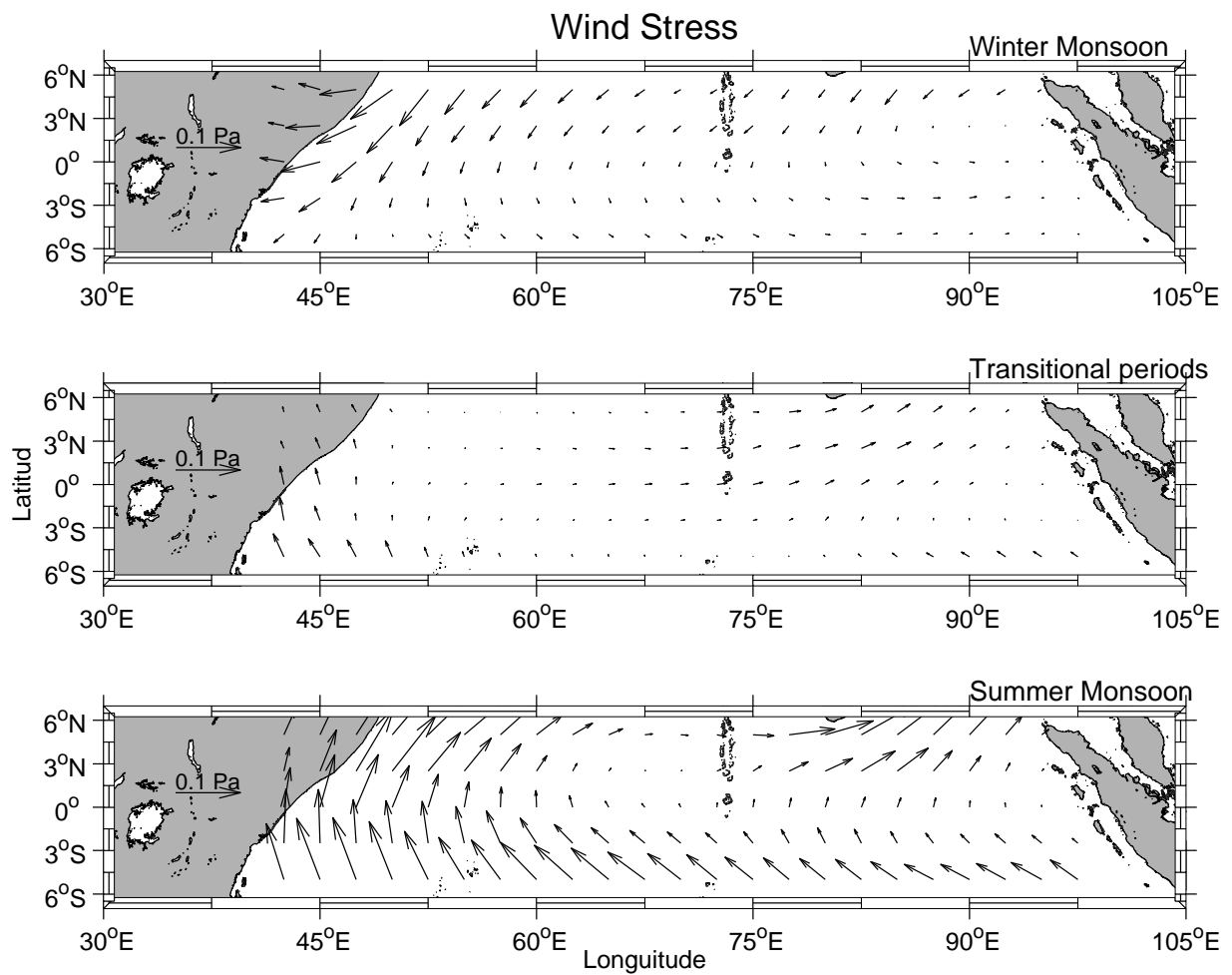


FIG. 1. Wind stress field in the Winter Monsoon (top), Transitional periods (middle) and Summer Monsoon (bottom).

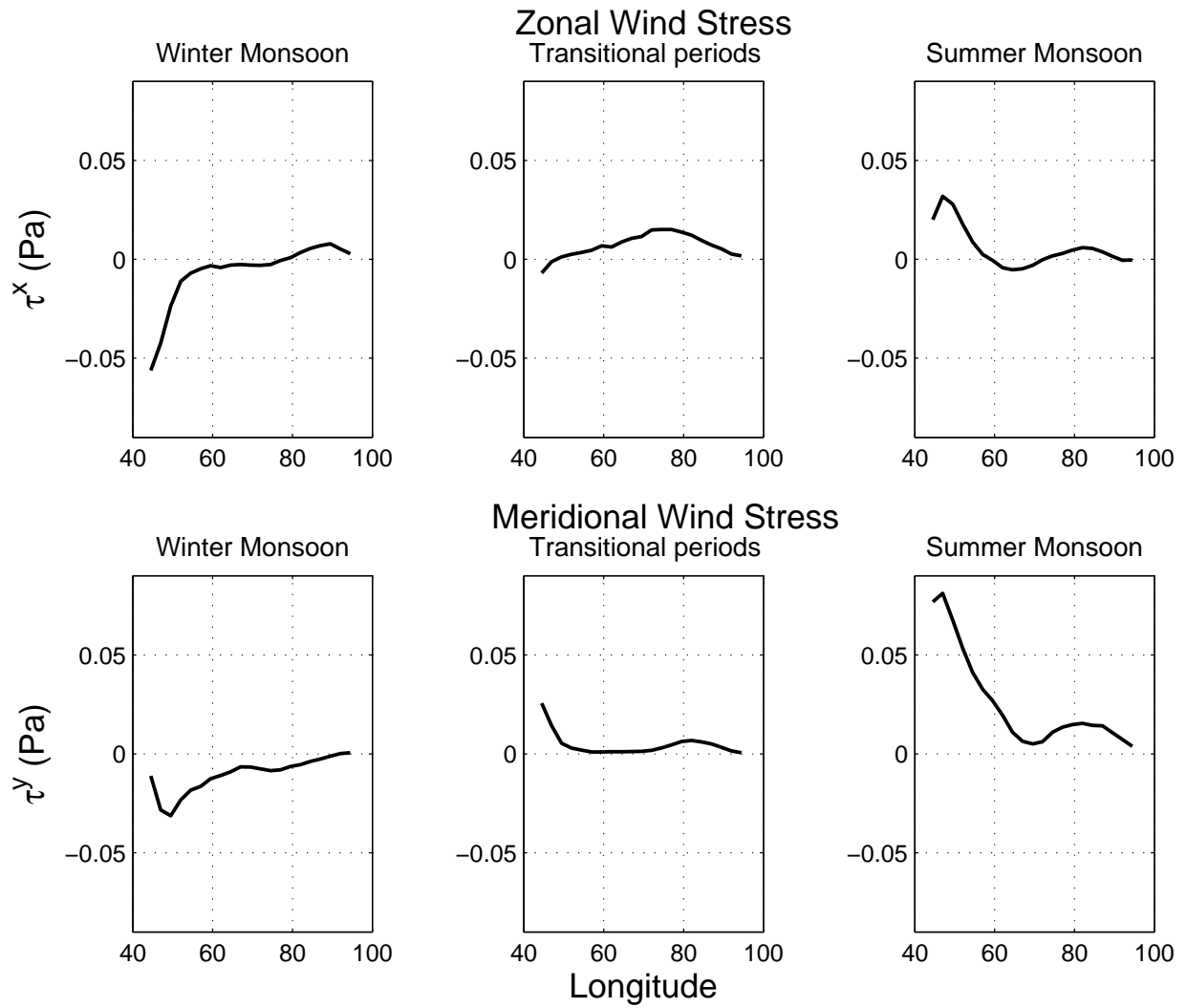


FIG. 2. Zonal (top) and Meridional (bottom) wind stress at the Equator in the Winter Monsoon (left), Transitional Periods (middle), and Summer Monsoon (right)

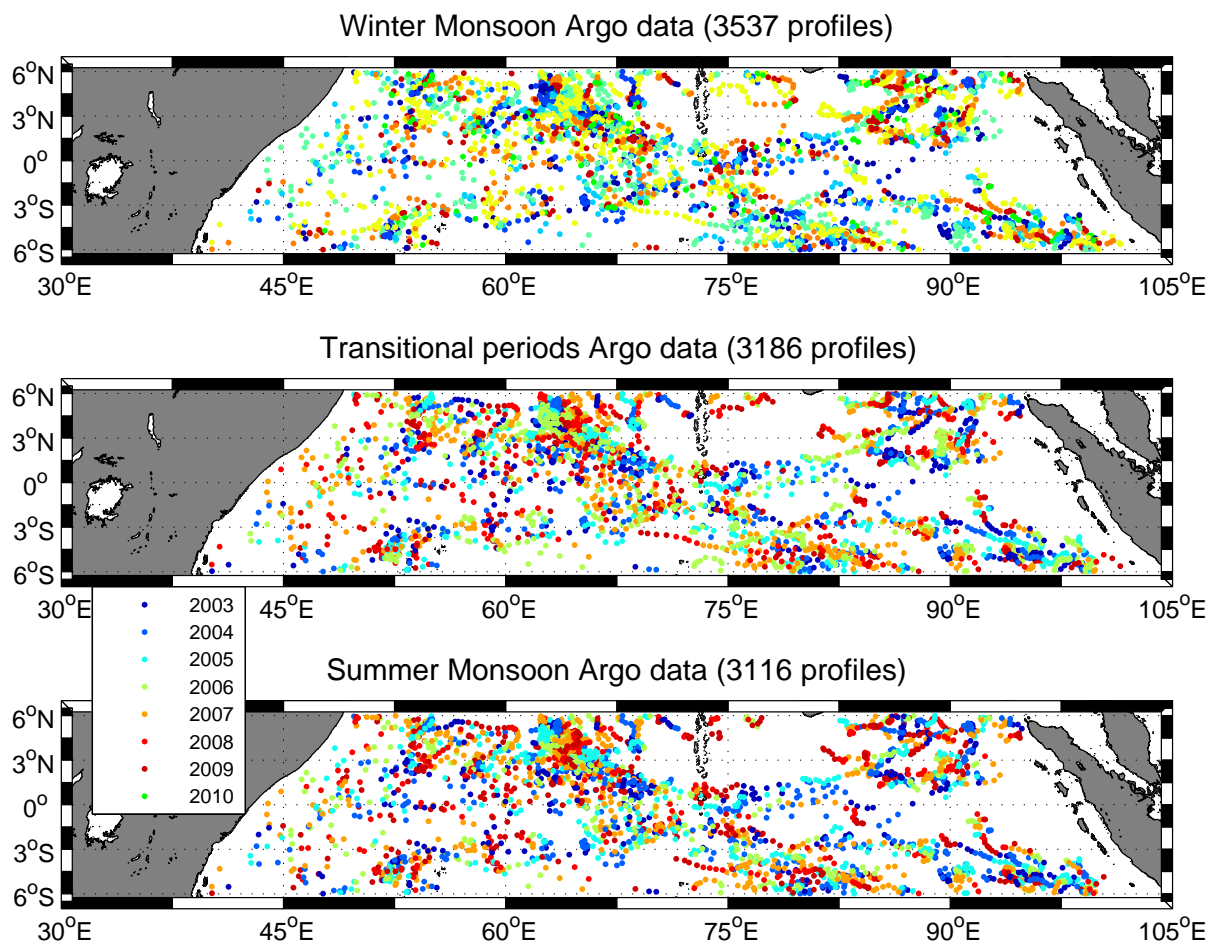
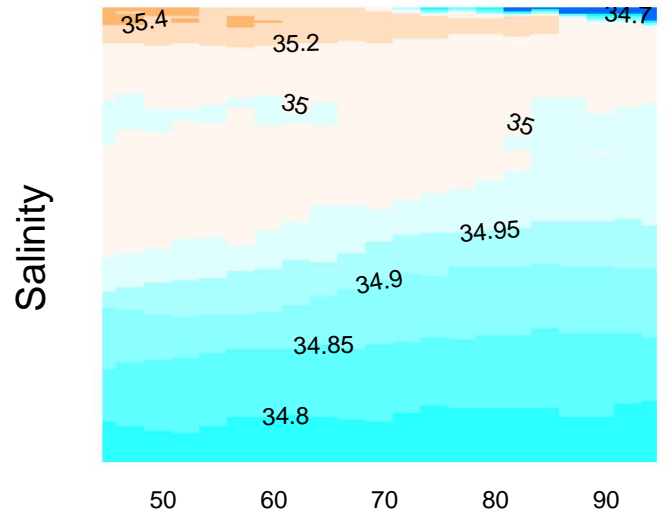
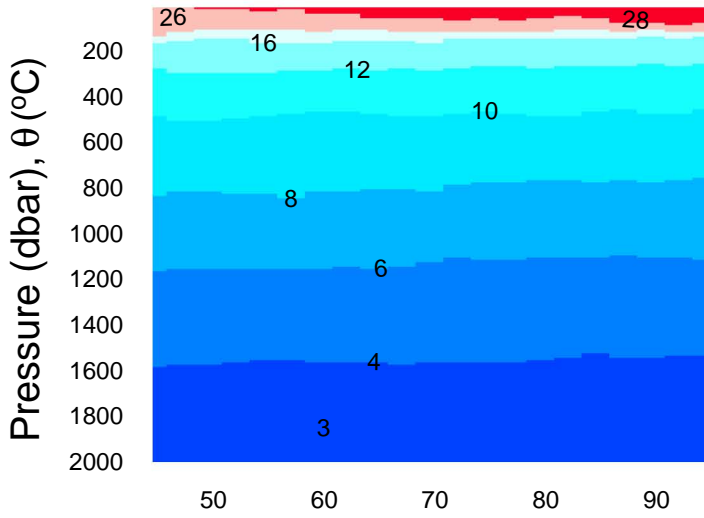
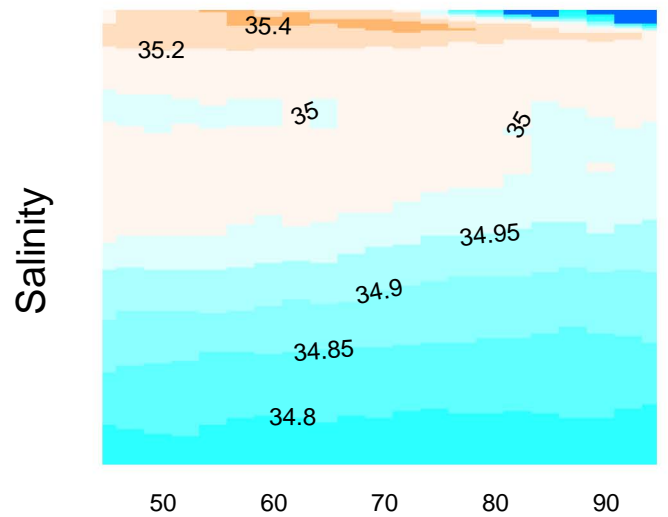
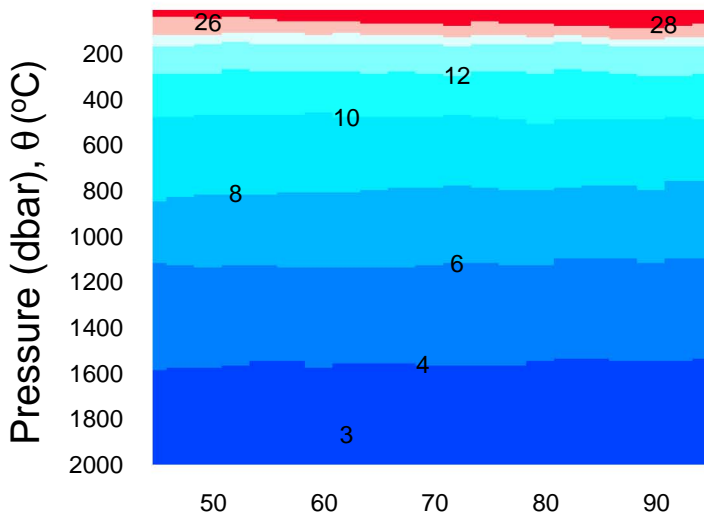


FIG. 3. Distribution of Argo floats over the equatorial Indian Ocean in each season. Colors represent the year of each profile.

WINTER MONSOON



TRANSITIONAL PERIODS



SUMMER MONSOON

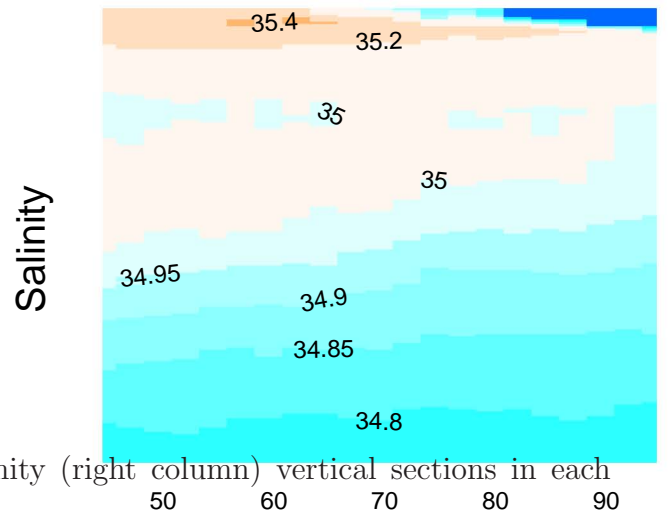
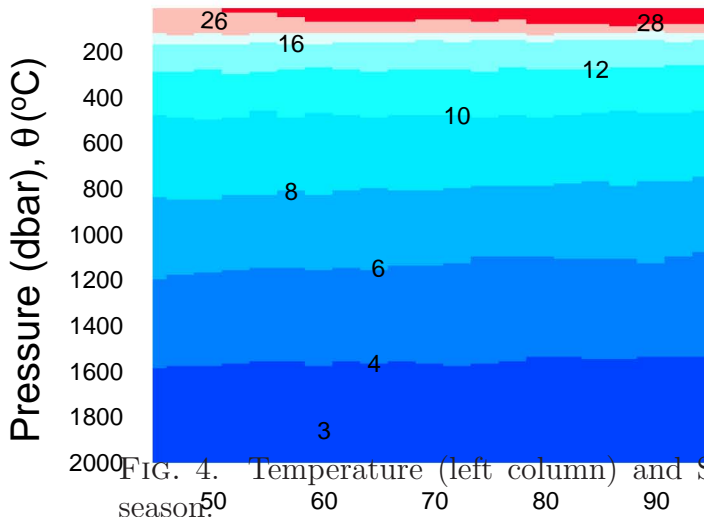
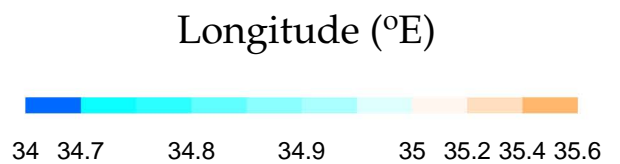
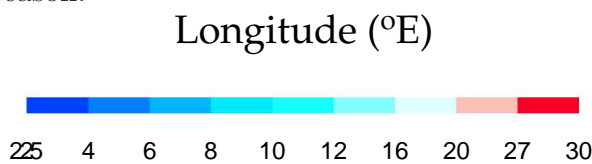


FIG. 4. Temperature (left column) and Salinity (right column) vertical sections in each season.



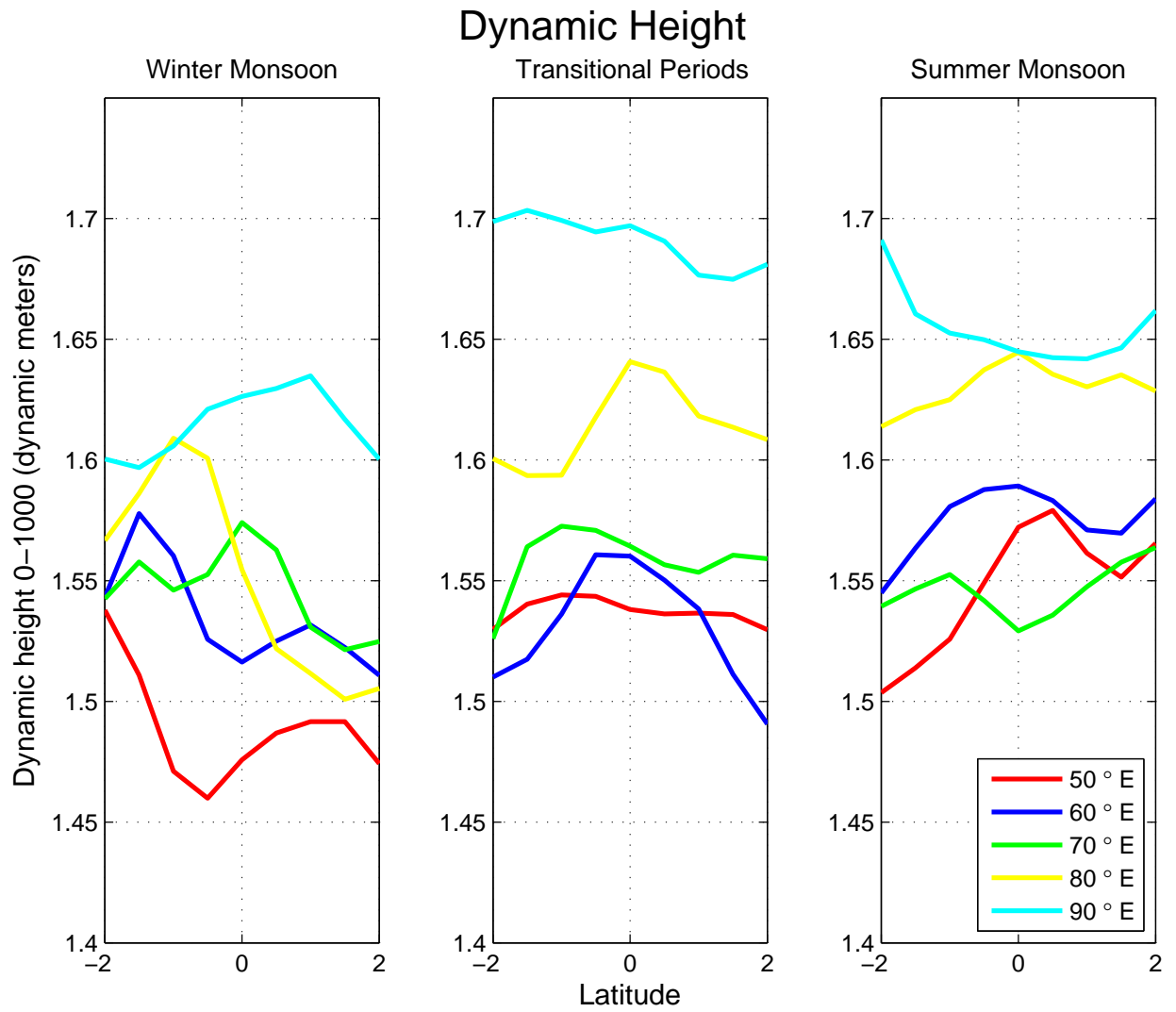


FIG. 5. Surface dynamic height relative to 1000 m depth (in dynamic meters) at selected longitudes across the equatorial Indian Ocean for each season.

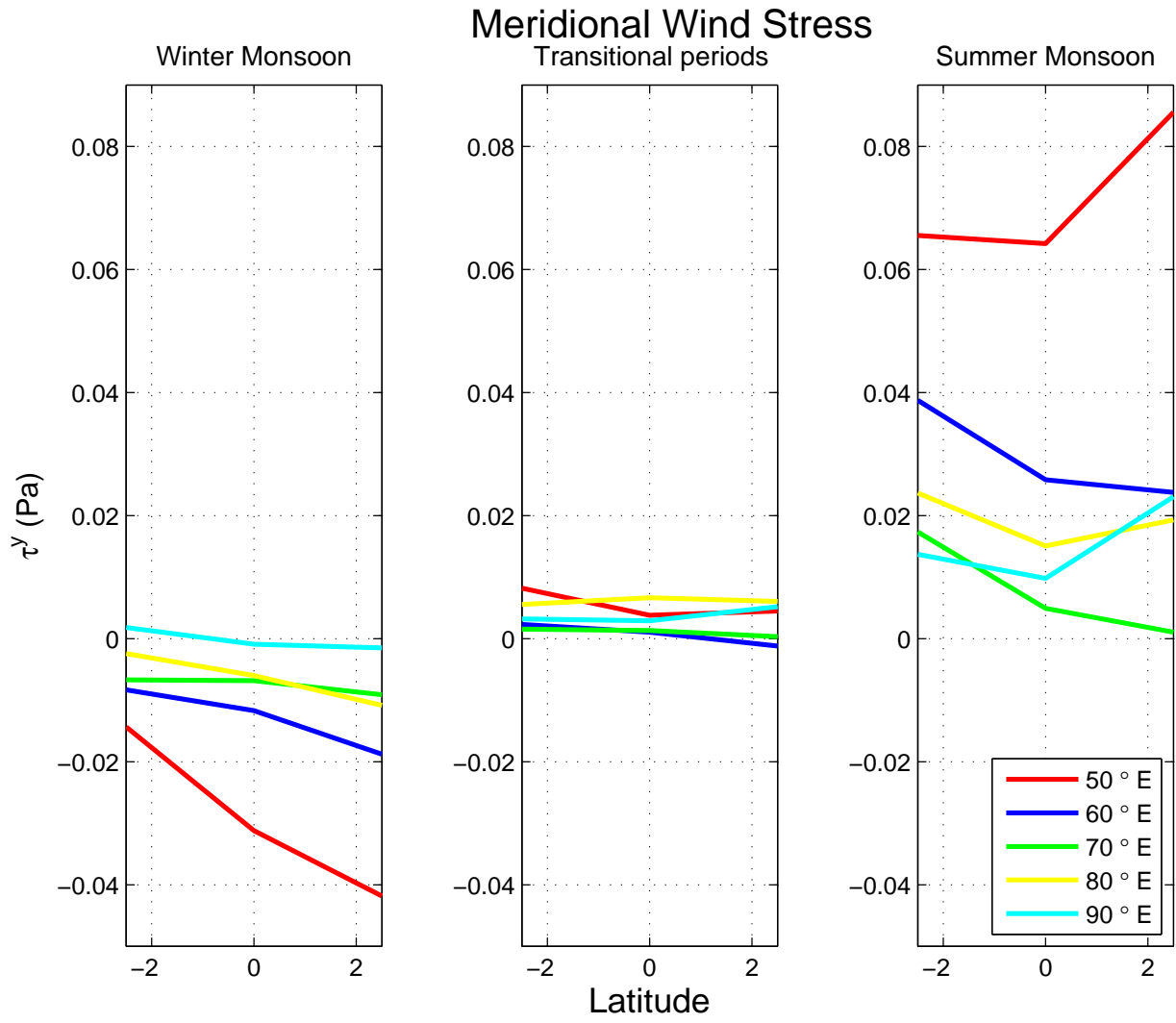


FIG. 6. Meridional wind stress (in Pa) at selected longitudes across the equatorial Indian Ocean for each season.

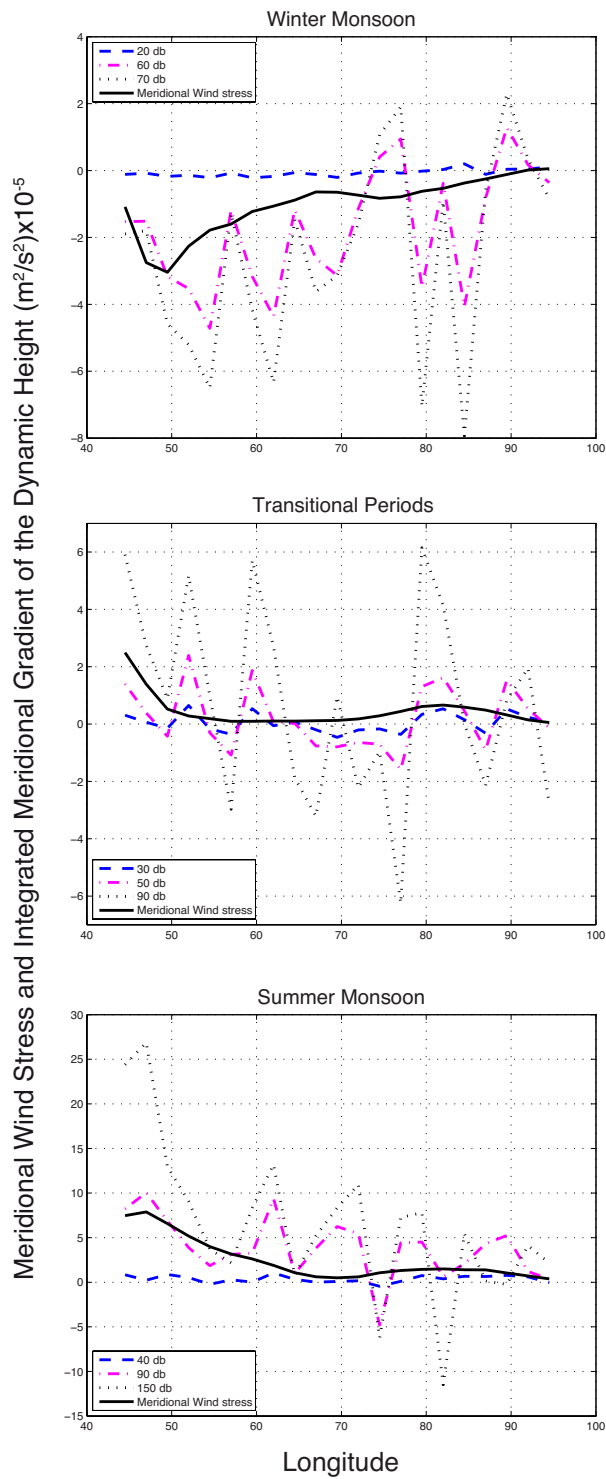


FIG. 7. Meridional wind stress (solid line) and integrated meridional gradient of the dynamic height at different pressure references (dashed lines) along the equatorial Indian Ocean. Each season has a different y-scale and pressure references.

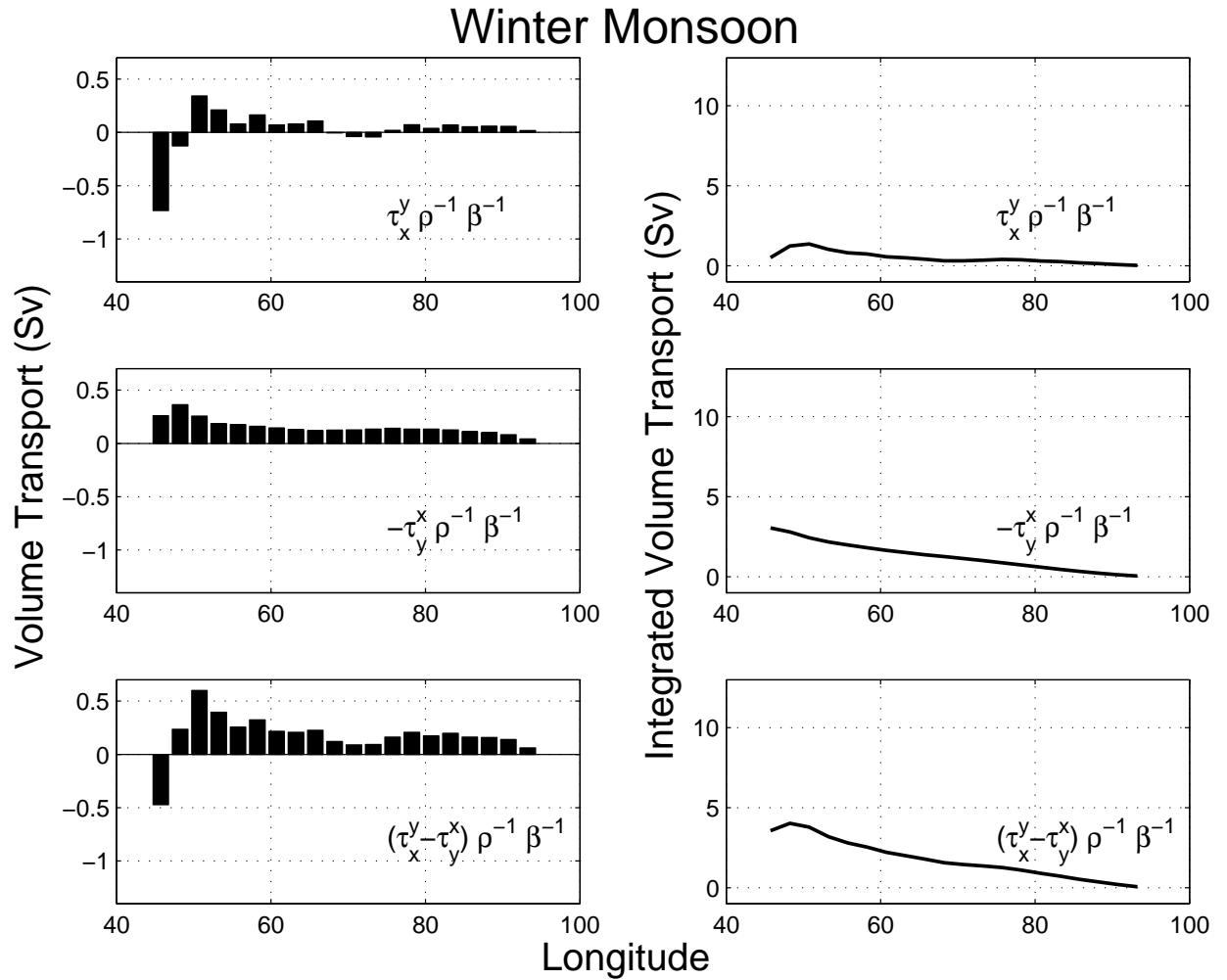


FIG. 8. Zonal distribution (left) and accumulated from the eastern boundary (right) volume transport of each component of the wind stress curl and total corresponding to the Winter Monsoon.

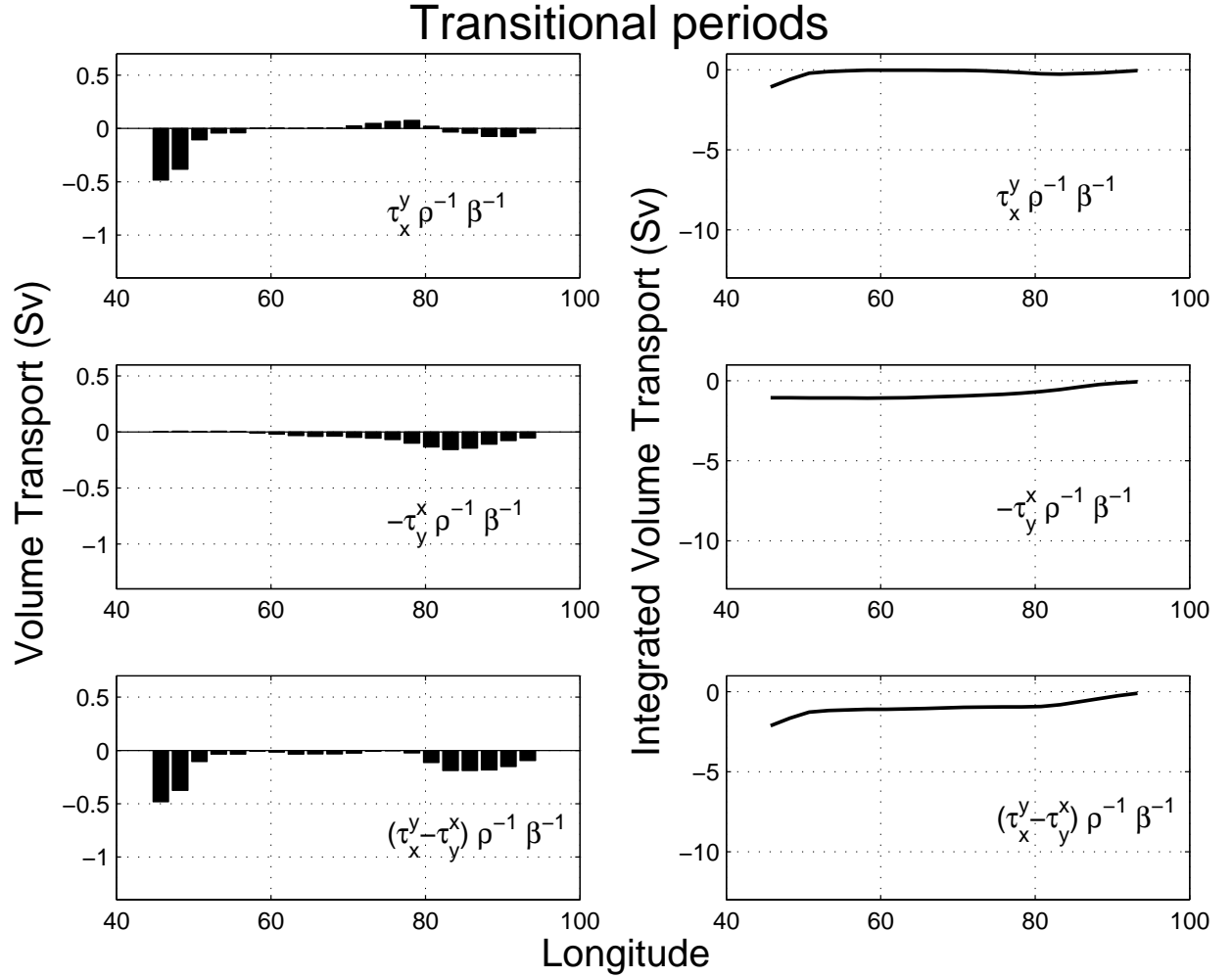


FIG. 9. Zonal distribution (left) and accumulated from the eastern boundary (right) volume transport of each component of the wind stress curl and total corresponding to the Transitional Periods.

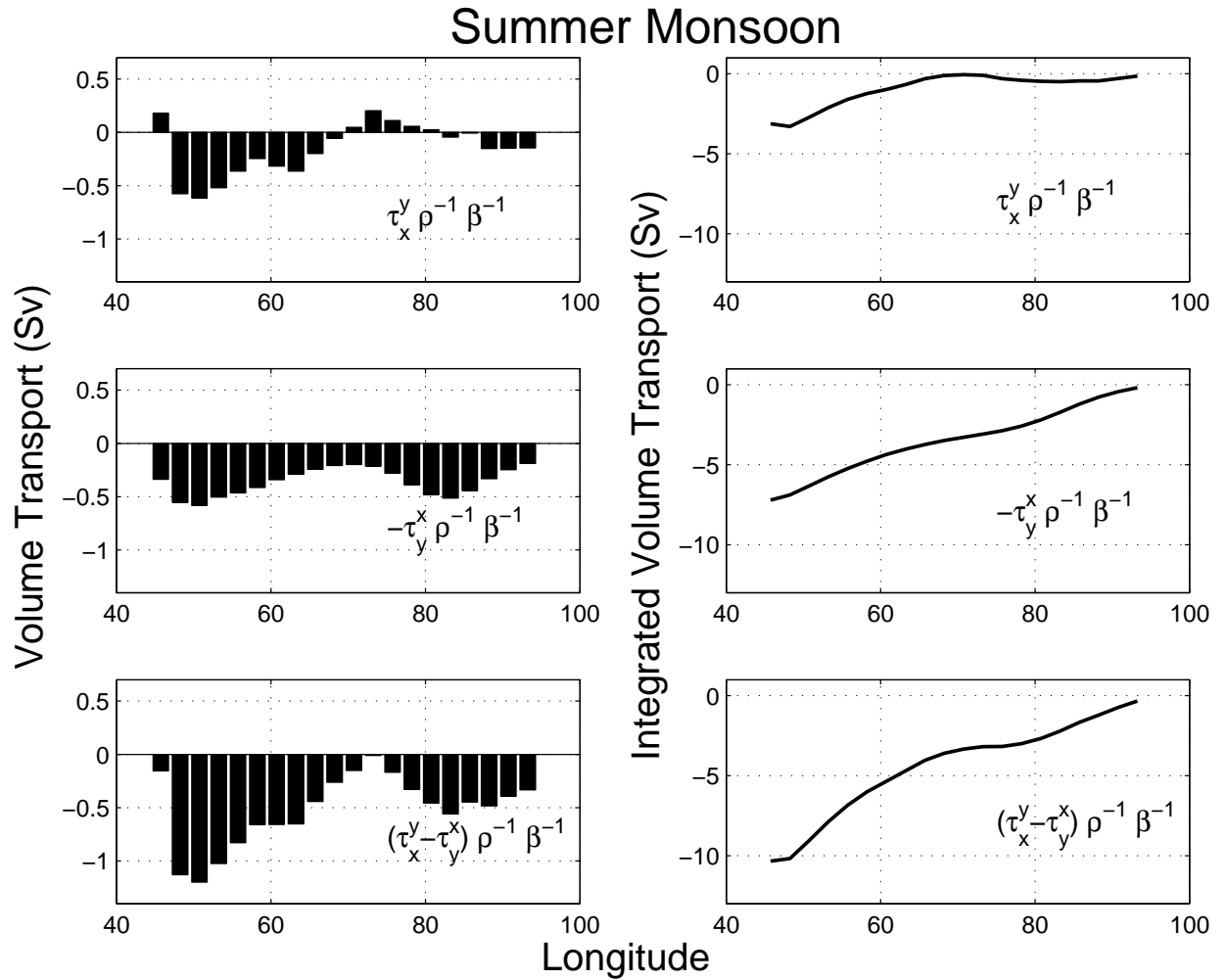


FIG. 10. Zonal distribution (left) and accumulated from the eastern boundary (right) volume transport of each component of the wind stress curl and total corresponding to the Summer Monsoon.

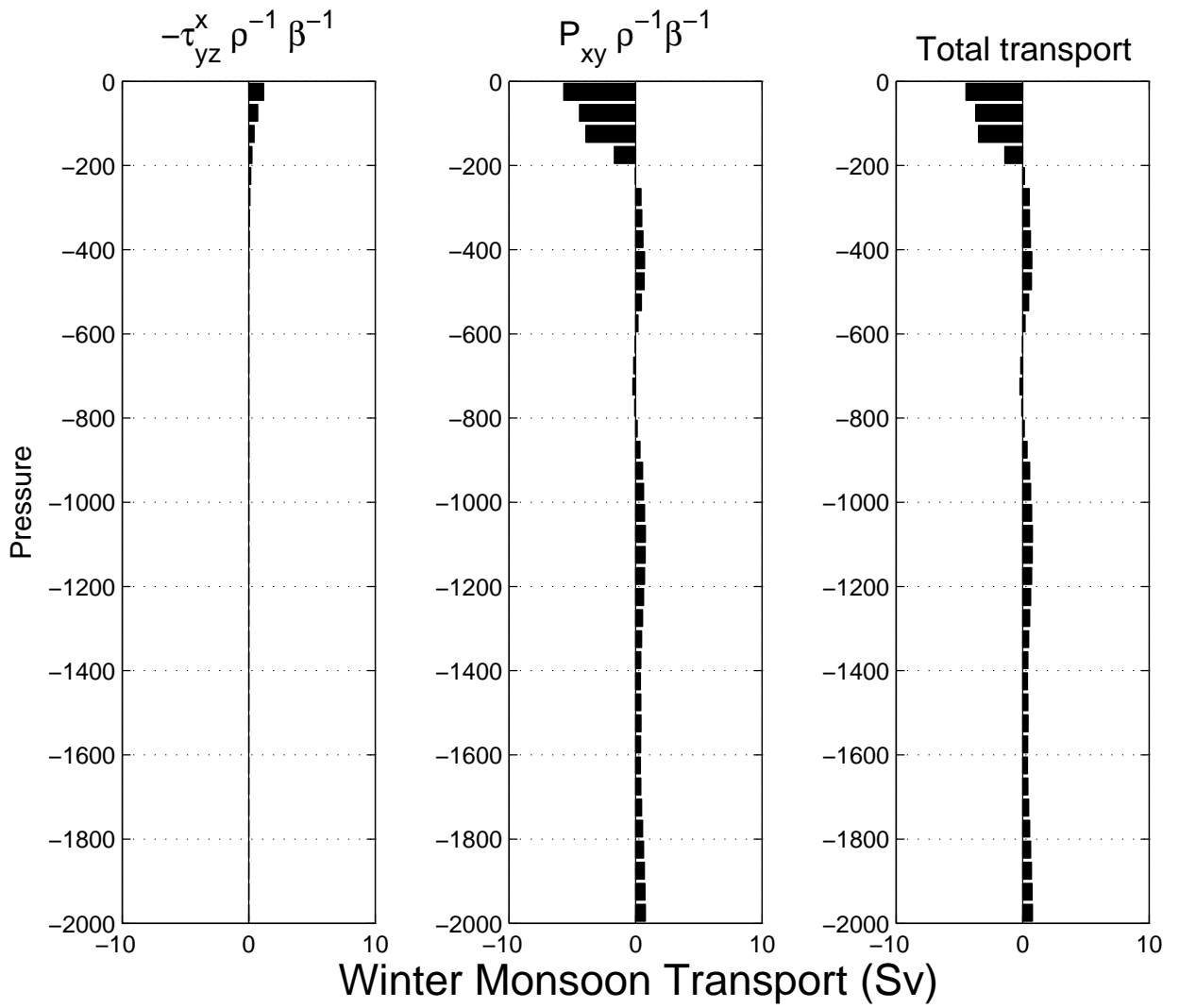


FIG. 11. Zonal integral of the volume transport from the surface to 2000 dbar every 50 dbar for $-\tau_{yz}^x$ (left), P_{xy} (middle) and total (right) for the Winter Monsoon.

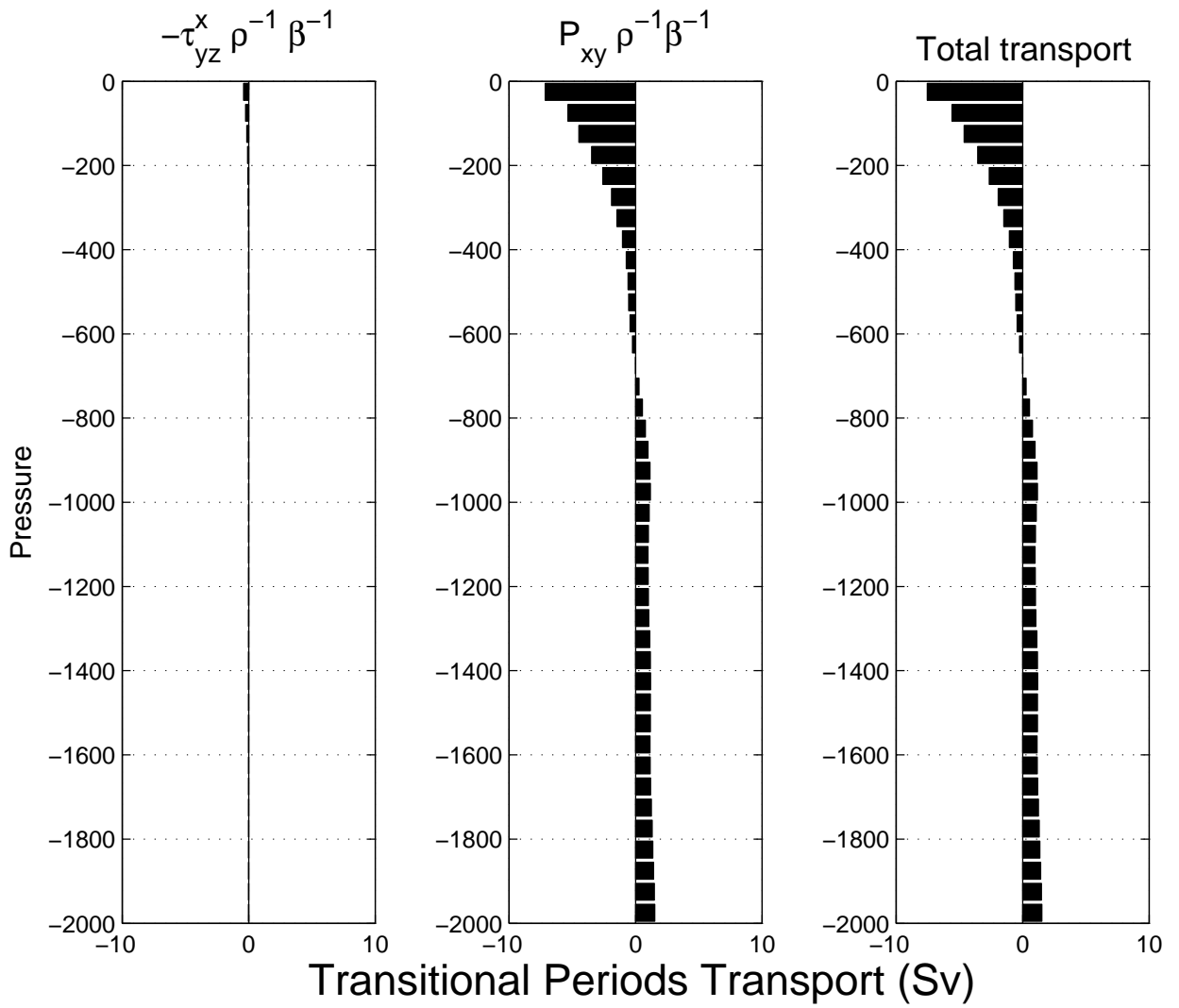


FIG. 12. Zonal integral of the volume transport from the surface to 2000 dbar every 50 dbar for $-\tau_{yz}^x$ (left), P_{xy} (middle) and total (right) for the Transitional Periods.

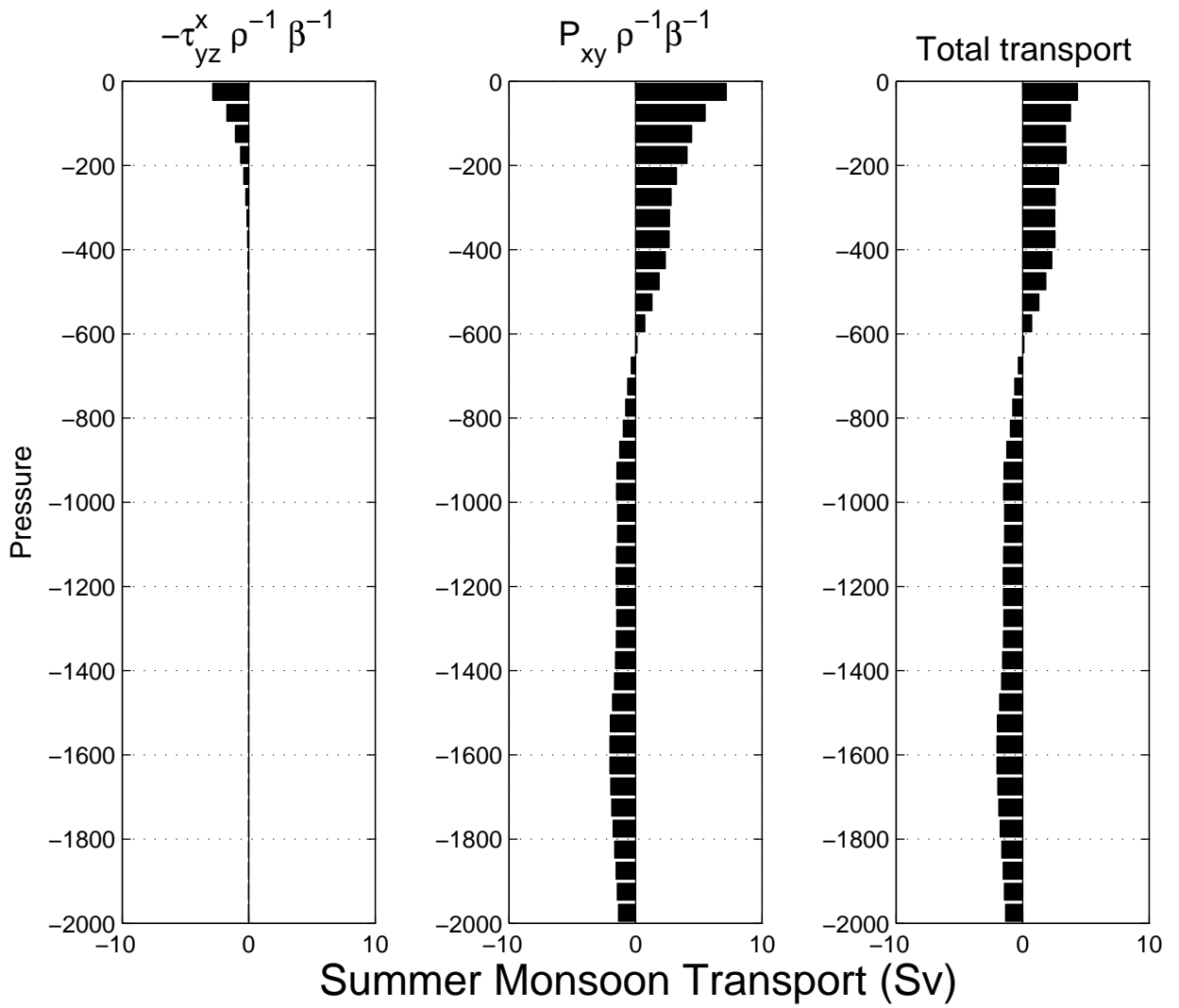


FIG. 13. Zonal integral of the volume transport from the surface to 2000 dbar every 50 dbar for $-\tau_{yz}^x$ (left), P_{xy} (middle) and total (right) for the Summer Monsoon.

Meridional Velocity (cm/s) Winter Monsoon

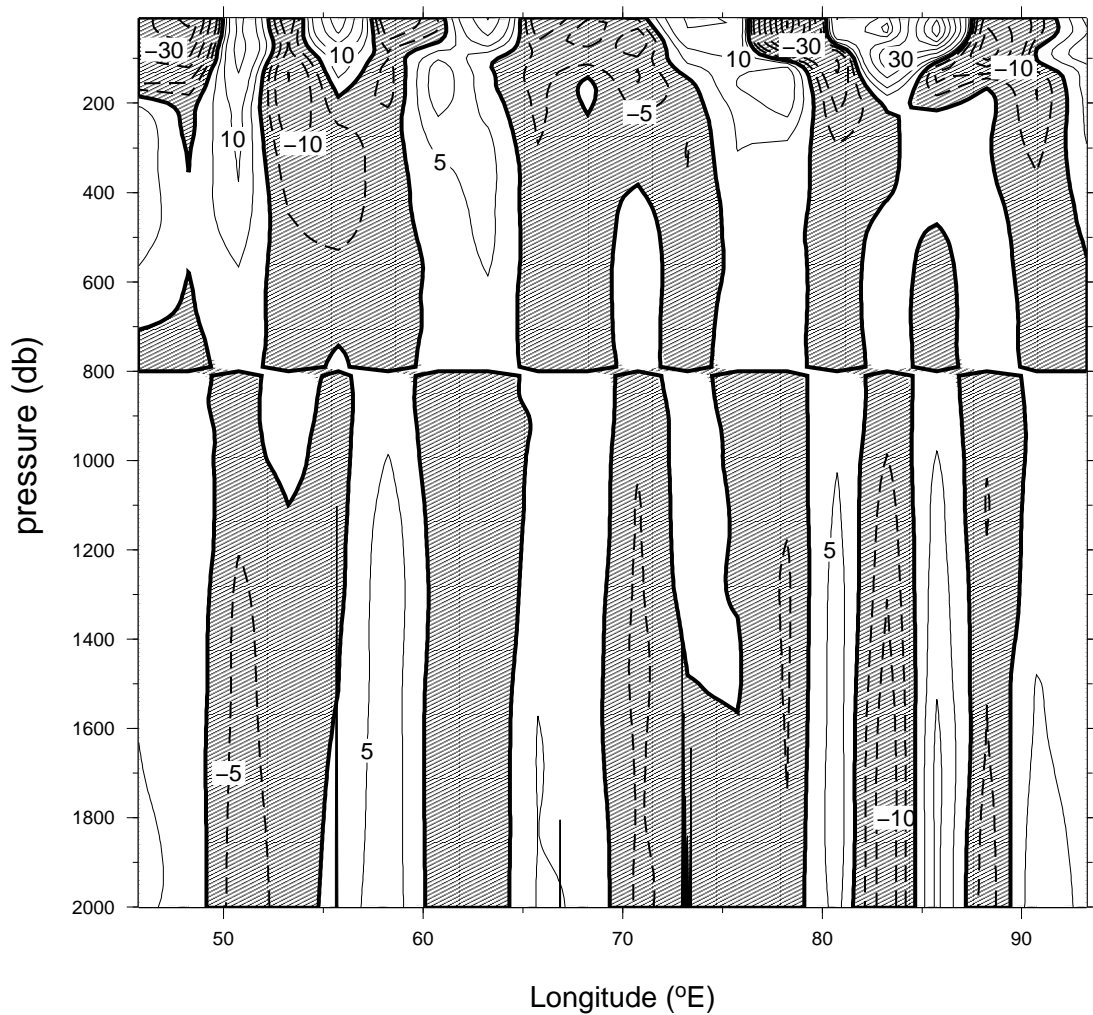


FIG. 14. Vertical section of meridional velocities (in $cm\ s^{-1}$) at the equatorial Indian Ocean in the Winter Monsoon. Negative velocities are cross-hatched. The isolines interval is 5 to $10\ cm\ s^{-1}$ and $10\ cm\ s^{-1}$ afterwards.

Meridional Velocity (cm/s) Transitional Periods

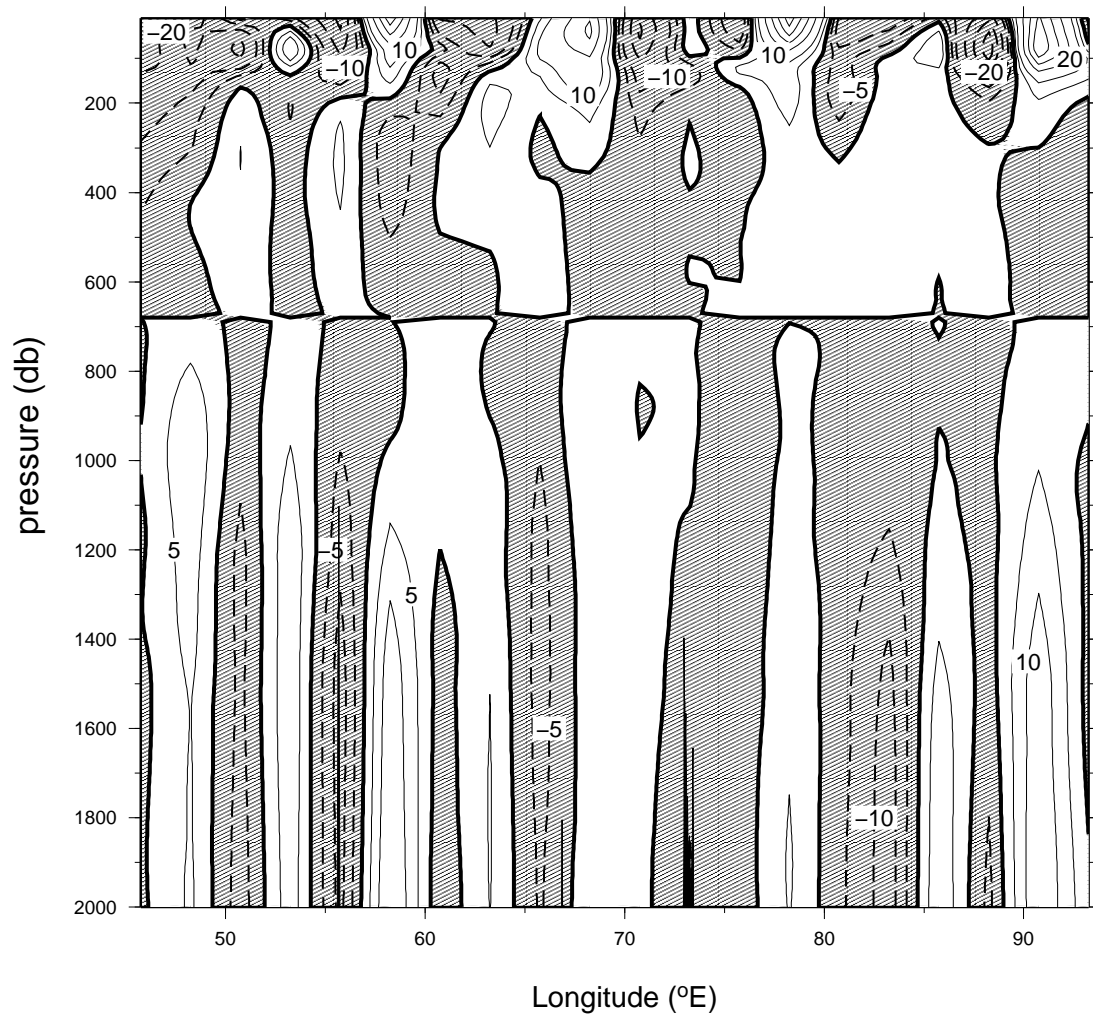


FIG. 15. Vertical section of meridional velocities (in $cm\ s^{-1}$) at the equatorial Indian Ocean in the Transitional Periods. Negative velocities are cross-hatched. The isolines interval is 5 to $10\ cm\ s^{-1}$ and $10\ cm\ s^{-1}$ afterwards.

Meridional Velocity (cm/s) Summer Monsoon

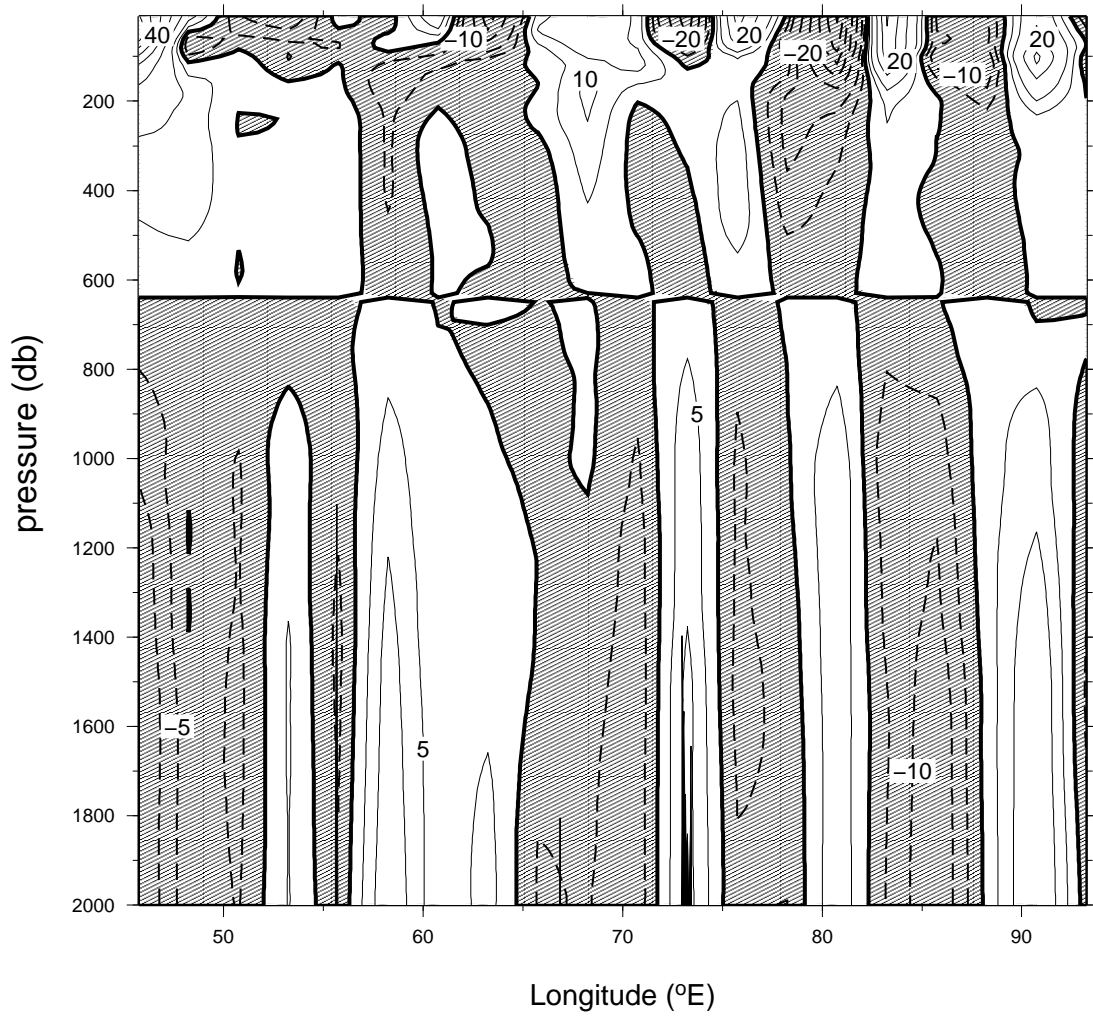


FIG. 16. Vertical section of meridional velocities (in $cm\ s^{-1}$) at the equatorial Indian Ocean in the Summer Monsoon. Negative velocities are cross-hatched. The isolines interval is 5 to $10\ cm\ s^{-1}$ and $10\ cm\ s^{-1}$ afterwards.